Monodisperse Draft

Jari Kolehmainen

October 15, 2015

Abstract

1)We propose a way to solve the arbitraty Youngs modulus effects on the charge transfer by stiffness scaling.
2)This is the first study combining tribocharging, electrostatics of granular materials, and fluidization. Earlier fluidization studies concentrated to bubbling fluidized beds.
3)The time needed for a fluidized bed to reach uniformly charged state is very long.
4)There is a nonuniform charge distribution inside the fluidized bed.
5)The wall tends to become couted with highly charged particles.
6)The particle charging effects the bed height oscillations, and in certain cases the bed expansion.
7)The slugging behavior of the fluidized bed was changed in a complex way with increasing particle charging.

1 Introduction

It has been known for centuries that during a mechanical contacts materials may develop static charges. This phenomenon is observed when one rubs a balloon against wool cloth, and observes the balloon sticking to the cloth and is known as tribocharging. It has also been known for decades that granular material in transport lines and fluidized beds tend to create charges [12]. This charging may cause spark generation leading even to powder explosions [10]. Triboelectric charging is generally been considered unwanted phenomenon, such as particle wall fouling in polyethylene reactors [6], but is also crucial in certain applications such as photocopying and laser printing where toner particles are charged via triboelectric charging.

Triboelectric charging is still very poorly understood phenomenon and multiple different mechanism have been proposed for this in past decades [12]. The most widely cited mechanism for the tribocharging is electron transfer [4], where the charge transfer is believed to happen due to electrons transfering from material surface to another material surface. While this mechanism is found to be in good agreement with experiments for metals, there is some debate weather it is applicable to insulators [15].

In electron transfer model materials tendency to pick up charges is described by a work function value. For metals this work function value is defined as the energy needed to remove one electron form the metal surface [4]. For insulators this work function value correlates poorly with the tribocharging behavior, and instead effective work function value is often used to describe the charging behavior of insulators in numerical simulations [14]. Unfortunately, there is no direct way to measure the effective work function value due to its vague definition.

Moreover, it is well-known that the triboelectric charging of insulators depends on the ambient humidity [3] and on the particle size [17, 2, 18]. It is not straght forward to determine these effects and the effective work function would need to modelled for these parameters. There has also been more direct simulation approaches to take the insulator charge size dependency into account by modelling the electrons on the particle surface [1] or by introducing high and low energy electrons [11]. While these models can capture the size dependency to some extent, it is hard to incorporate charge transfer of different materials into these models. Furthermore, modelling the electrons in the particle surface is computationally very demanding and not suitable for fluidized bed simulations with more than thousand particles.

It was proposed in [13] that the effective work function value could

be determined from macroscopic charging behavior. Laurentie et. al. charged the particles by a vibrated bed, and determined run series of simulations with various effective work function values to match the simulations and experiments. The determined work function value was validated by similar experiments, and the results showed very good agreement. For these reasons, this study will also base the triboelectric charging behavior to effective work functions as they seem a promising tool for simulating triboelectric charging.

There has been multiple studies concentrating in electrostatic effects on fludized beds. Earlier computational studies were based on Eulerian-Eulerian simulations that model the solid and gas phase as continuum [16, 8]. These studies assumed constant charge on particles, and solved the electric field by solving a Poisson equation for electric potential. If the permittivity of the varying solid content is taken into account the large scale electric field can be solved accurately [16]. These studies found that the electrostatics altered the bubbling behavior of fluidized beds by squeezing bubbles at the center of the bed [16, 7, 9].

The shortcoming of the Eulerian-Eulerian approach is that it require additional modeling for particle drag and particle stresses since the local electrostatic effects may alter these parameters. These local effects have not been addressed in any of these simulations. Furthermore, it is not easy to simulate non uniform charge distributions with Eulerian-Eulerian simulations. To overcome this recent article [5] simulated bubbling fluidized bed by employing four-way-coupled CFD-DEM simulations that model particles individually, and use Eulerian modeling for the solid phase. The study used also predefined charges on particles and considered both monodisperse (same charge on all the particles) and bidisperse case where particles had different prefixed charges.

In the article [5] concluded that the bubble size decreased with introduction of charge on particles in mono charged case that is in-line with the Eulerian studies of Jalalinejad [8, 7, 9]. In the bidisperse case, the oppositely charged particles formed chains inside the bubbling bed, and interestingly caused the bubbles that were similar to the neutrally charged case.

The aim of this study is to inspect the interplay between the triboelectric charging and electrostatic effects. The triboelectric model chosen was similar to [13] while the electrostatic force was modelled in a similar way to [5]. The fluidization regime was chosen slightly above the bubbling regime as its more relevant for polyethylene reactors.

2 Computational Model

2.1 Overview

2.2 Hydrodynamic Model

2.3 Triboelectricity and Electrostatics

The electrostatics were introduced to the simulation by allowing particles to experience triboelectric charging. The triboelectric charging was based on an effective work function model that characterized triboelectric charging tendency of each material by an effective work function ϕ.

The charge transfer rate during a collision is given by

$$\frac{dq}{dt} = H\left(\frac{dA}{dt}\right)\frac{dA}{dt}\frac{\varepsilon}{\delta_c e}\left(\Delta\phi + \mathbf{E}_{ij}\cdot\mathbf{n}_{ij}\delta_c e\right), \tag{1}$$

where A is the contact area, $H(\,\cdot\,)$ is Heaviside function, δ_c is the maximum distance where the charge can transfer from object to object, typically taken to be 500nm, e is the charge of an electron, ε is the electric permittivity, and $\mathbf{E}_{ij}$ is the electric field at the contact point.

The Heaviside function is used to stop the charge transfer back to where it came from. It is generally accepted that there is some level of charge relaxation happening when particles are coming apart that is neglected in the Eq. (1). However, there is no prior work or model to determine this backflow of charge, and it will be neglected in this study. Therefore, the Eq. (1) will slightly overestimate the charge transfer between the particles.

The electron field at the contact point was computed from the neighboring particles that included also the colliding particles by direct sum

$$\mathbf{E}_{ij} = -\frac{1}{4\pi\varepsilon}\sum_k \frac{q_k\mathbf{r}_k}{\|\mathbf{r}_k\|^3}, \tag{2}$$

where $\mathbf{r}_k$ is vector pointing from k:th particles center to the center of the contact. The neighboring particles are defined by setting a cut-off radius for the electrostatic interactions. Any particles that are further than the predefined cut-off radius are neglected from the sum.

During the simulation the charge transfered between the particles i and j between timesteps n and $n+1$ becomes

$$\Delta q^{n+1} = H(\Delta A)\Delta A\frac{\varepsilon}{\delta_c e}\left(\Delta\phi - \mathbf{E}_{ij}^n\cdot\mathbf{n}_{ij}\delta_c e\right), \tag{3}$$

where the electric field $\mathbf{E}_{ij}^n$ is evaluated at the previous time step n, and ΔA is the change of contact area between the timesteps. The transfered charge Δq^{n+1} is typically small, and the stiffness of the Eq. (1) does not become an issue with timesteps typically used for the soft sphere model. The good sides of the triboelectric model of Eq. (1) is that it can capture collisions of different materials, the effect of surrounding electric field, and the effect of contact force via the contact area. The subtle physics can be introduced by making the effective work function ϕ as a function of various parameters such as particle size or ambient humidity.

The electrostatic force on a particle was evaluated as

$$\mathbf{F}_i = q_i \mathbf{E}(\mathbf{x}_i), \tag{4}$$

where q_i is the charge of the particle, $\mathbf{x}_i$ is the location of the i:th particle, and $\mathbf{E}(\mathbf{x}_i)$ is the electric field at the particles location. The electric field is evaluated from neighboring particles as before by the pairwise summation

$$\mathbf{E}(\mathbf{x}_i) = -\frac{1}{4\pi\varepsilon} \sum_{k \neq i} \frac{q_k(\mathbf{x}_k - \mathbf{x}_i)}{\|\mathbf{x}_k - \mathbf{x}_i\|^3}. \tag{5}$$

In our simulations each particle presented individual particles and not collection of particles like in parcel simulations, hence no screening is needed in Eq. (5).

2.4 Effects of Particle Stiffness

Recall that the charge transfer of a particle during a collision is given by

$$\frac{dq}{dt} = H\left(\frac{dA}{dt}\right) \frac{dA}{dt} \frac{\varepsilon}{\delta_c e} \left(\Delta\phi - \mathbf{E}_{ij} \cdot \mathbf{n}_{ij} \delta_c e\right), \tag{6}$$

where $\mathbf{E}_{ij}$ is electric field in the contact point, and $\Delta\phi$ is the work-function difference. The electric field in the contact point will depend on the particles charge. Therefore, the right hand side of Eq. (6) will depend on the particles charge. The Eq. (6) can be written in terms of particles charge transfered by splitting the charge to initial charge q_0 and denoting the transfered charge by q. In particular, we have $q(0) = 0$ as at the beginning of contact no charge is transfered. This allows us to write

$$\frac{dq(t)}{dt} = \frac{dA}{dt} \left(\beta - \alpha q(t)\right), \tag{7}$$

where α is a qeometrical coefficient depending only on particle radius, and β is coefficient depending on the collision type (wall or other particle) and initial charge(s). The detailed formulas for α and β are given in the appendix. Solving the ODE (7) for q with initial condition $q(0) = 0$ and $A(0) = 0$, and assuming that the contact area is independent function of charge $q(t)$ yields

$$q(t) = \alpha\beta \left(1 - e^{-\alpha A(t)}\right). \tag{8}$$

Let $t = T$ be time where contact area $A(t)$ obtains its maximum value A_{max}. Inserting now $t = T$ to Eq. (8) yields charge transfered during one collision

$$\Delta q = \alpha\beta \left(1 - e^{-\alpha A_{max}}\right). \tag{9}$$

For typical collisions in a fluidized bed we have $A_{max} \ll \pi r_{eff}^2$ where r_{eff} is the effective radius of the Hertzian model. This yields $\| - \alpha A_{max}\| \ll 1$. Proof of this is given in the appendix. Invoking Taylors series expansion for $\exp(-\alpha A_{max})$ and neglecting higher order terms gives

$$\Delta q = \alpha^2 \beta A_{max}. \tag{10}$$

The ratio between charge transfer of a real and simulated soft particle is therefore,

$$\frac{\Delta q^{real}}{\Delta q^{soft}} = \frac{\beta^{real} A_{max}^{real}}{\beta^{soft} A_{max}^{soft}}. \tag{11}$$

To tackle the problem of soft particles againts the real hard particles we assume for time being that the maximum area is independent on the coefficient of restitution with. Setting coefficient of restitution to one allows us to inspect the energy balances of the collision. The potential energy of Hertzian spring is given by

$$E_p = \int F d\delta = \frac{8}{15} Y_{eff} \sqrt{r_{eff}} \delta^{5/2}, \tag{12}$$

where Y_{eff} is the effective Youngs modulus, and δ is the overlap distance. The overlap distance is connected to contact area by

$$A = \pi r_{eff} \delta. \tag{13}$$

When the contact area obtains its maximum value we have

$$\frac{dA}{dt} = \pi r_{eff} \frac{d\delta}{dt} = \pi r_{eff} v_{\perp} = 0, \tag{14}$$

where $v_\perp$ is the normal velocity. Hence at the maximum contact area we have $v_\perp = 0$, and the normal kinetic energy is transformed totally to Hertzian springs potential energy and to potential energy of the electric field. Assuming that the potential energy of the electricfield is negligible to the springs potential at the maximum contact area energy yields $E_p = \frac{1}{2}mv_\perp^2$.

Solving for δ_{max} from Eq. (12) we obtain

$$\frac{A_{max}^{real}}{A_{max}^{soft}} = \left(\frac{Y^{soft}}{Y^{real}}\right)^{2/5} \left(\frac{v_\perp^{real}}{v_\perp^{simu}}\right)^2, \tag{15}$$

where Y stands for particles Youngs modulus. The initial collision velocities may change slightly due to Youngs modulus, but are assumed to depend mainly on the hydrodynamics and the overal charge, hence we have $v_\perp^{real} \approx v_\perp^{simu}$. Hence, to correct the charge transfer in a single collision in a soft simulation one has to multiply the charge transfer by

$$\sigma = \frac{\Delta q^{real}}{\Delta q^{soft}} = \left(\frac{Y^{soft}}{Y^{real}}\right)^{2/5}. \tag{16}$$

Shifting our attention to particles charge over the total simulation time, and denoting that by $Q(t)$ we have

$$\frac{dQ(t)}{dt} = \omega(t)\Delta q(t), \tag{17}$$

where $\omega(t)$ is number of collisions per time unit, and Δq charge transfered during one collision that is obtained from Eq. (10). We assume here that the collision rate would be only function of time and particle parameters even it may depend on the charge in a complicated way.

As noted before $\Delta Q(t)$ depends on $\beta(t)$ and $v_\perp$ (now function of time as it depends on $Q(t)$) that is an affine function of the particles charge before each collision. Therefore we have

$$\frac{dQ(t)}{dt} = \omega(t)a\left(Q_{eq} - Q(t)\right), \tag{18}$$

where a is a coefficient that depends on $v_\perp$ and Younds modulus, and Q_{eq} is coefficient that depend only on the particles initial charge at the beginning of the whole simulation and on the imposed work functions. The exact values of the coefficients are given in the appendix and depend on the collision type. In particular coefficient a depends linearly on the maximum contact area, and Q_{eq} is independent on the Youngs modulus.

Solving again the familiar ODE (18) yields

$$Q(t) = Q_{eq}\left(1 - e^{-a\int \omega(t)dt}\right). \tag{19}$$

Assume that the maximum contact area of soft simulation would be multiplied by a number, say σ. Setting the right hand sides of Eq. (19) as equal for soft and hard particles, and after some algebraic manipulation we obtain

$$\sigma(t) = \left(\frac{Y^{soft}}{Y^{real}}\right)^{2/5} \left(\frac{v_\perp^{real}(t)}{v_\perp^{simu}(t)}\right)^2 \frac{\int_0^t \omega_{real}(\tau)d\tau}{\int_0^t \omega_{soft}(\tau)d\tau} \tag{20}$$

The Eq. (19) is valid if the charging does not affect the maximum contact area during one collision. The Eq. (19) has few implications. Firstly, to simulate a system of hard particles with soft particles it is enough to multiply soft particles contact area by coefficient given in Eq. (16) to obtain correct charging rate. This correction is valid as long as charges in the system are small enough not to alter the collision rate function $\omega(t)$. If the collision rate is changed the coefficient is given by Eq. (20).

The second implications is that if we have simulated a charging rate of a system with soft particles the results should be shown with time scaled by the coefficient of Eq. (20) or by a coefficient of Eq. (16) if the collision dynamics is not changed by the charging.

The proposed correction of Eq. (16) was tested in number of two particle collision with varying coefficients of restitution, Youngs modulus, and various initial velocities. The charge on the particles was fixed as $\pm 1.0^{-13}$C, and the work function difference was zero.

The uncorrected case is shown in Fig. 1 showing very different values of charge transfer. The same case was run again with corrected charge transfer, and the results are shown in Fig. 2. The corrected case shows very neat collapse of all the cases to the base case with Youngs modulus 10^8. The cases in Fig. 1 and 2 are computed with high coefficient of restitution 0.9 that is close to coefficient of restitution 1.0 assumed in our theoretical reasoning. We also tested the correction in lower coefficient restitution 0.3 case to see if the results still showed good agreement. The results are shown in Fig. 3, and the curves collapsed fully. In the very small velocity limit, the coefficient of restitution caused the particles to come at full stop. Suprisingly, the corrected charge transfer was still to correct value even the coefficient of restitution would dominate the collision in such case. In addition we also tested multiple particle simulations with wall with different Youngs modulus, namely 10^5 and 510^6, with the correction. The correction was taken respect to Youngs modulus 3×10^9 that corresponds to polyethylene. The results showed very good fit, and the

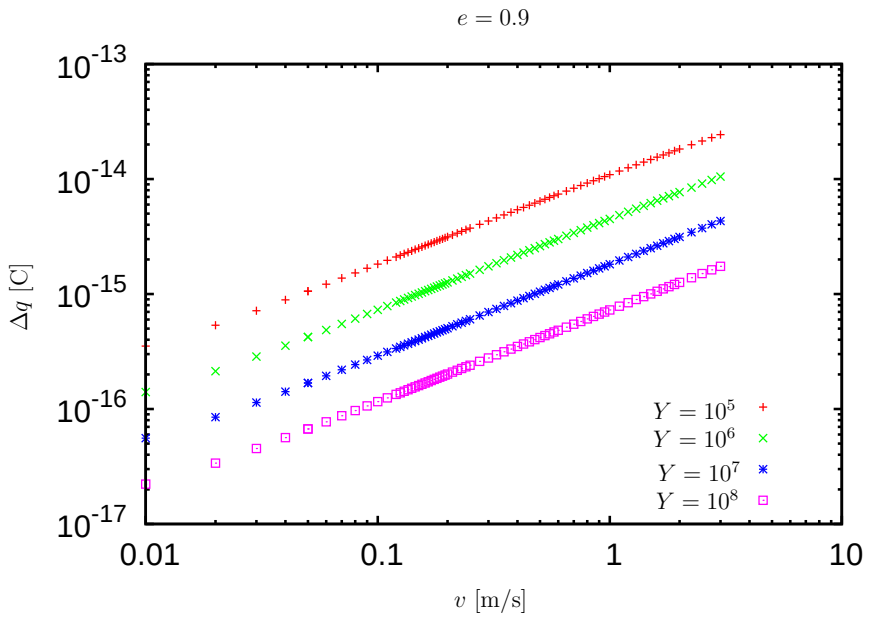

Figure 1: Figure showing charge transfer between two particles with coefficient of resitution 0.9, and with varying Youngs modulus and initial velocities. There is no correction employed to the charge transfer, and the results are widely different.

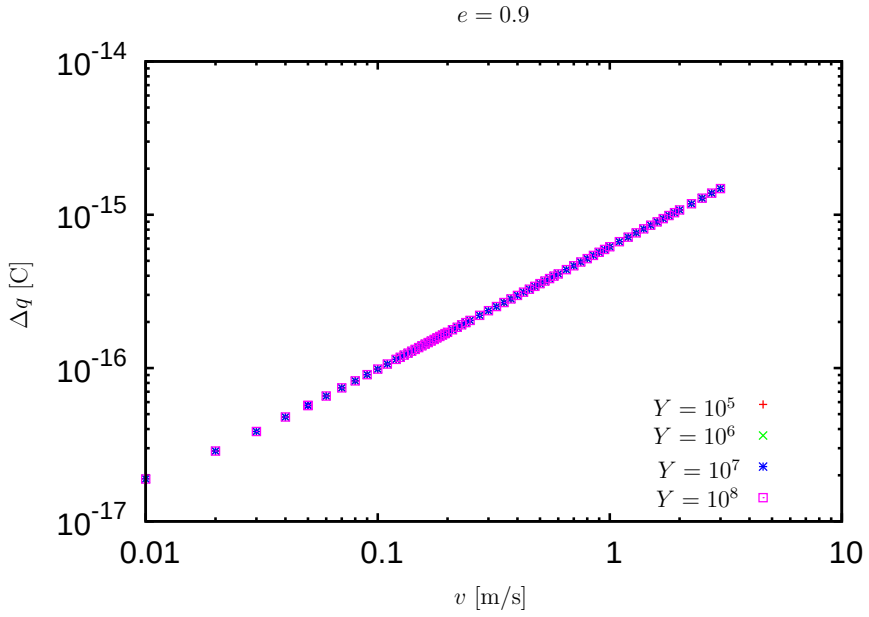

Figure 2: Figure showing corrected charge transfer between two particles with coefficient of resitution 0.9, and with varying Youngs modulus and initial velocities.

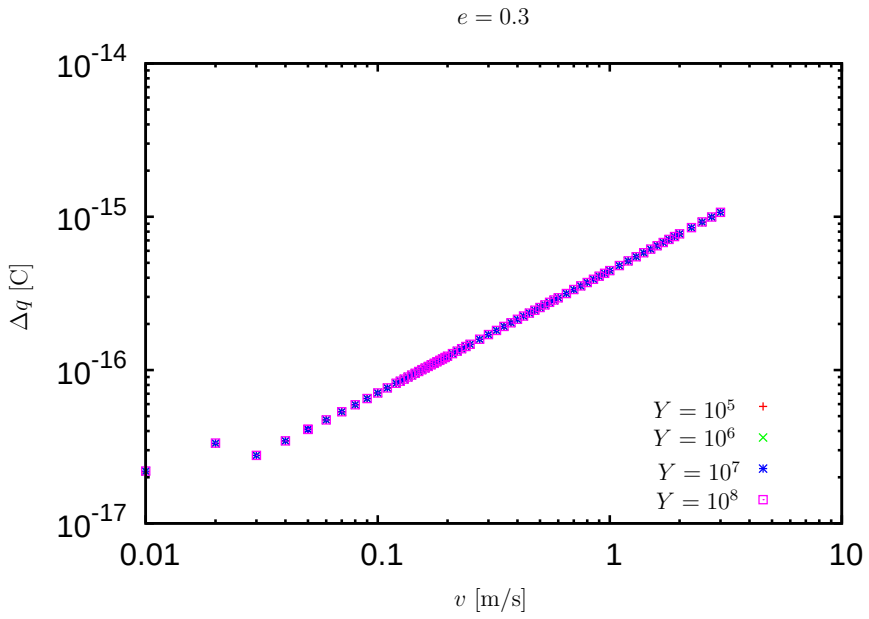

Figure 3: Figure showing corrected charge transfer between two particles with coefficient of resitution 0.3, and with varying Youngs modulus and initial velocities.

curves resembled each other exactly. This is not that suprising, since once the charging of each individual collision is captured accurately, the overall physics should remain the same.

3 Results

3.1 Overview

We simulated a slugging fluidized bed with various work function values and two different superficial velocities, namely $0.2V_t$ and $0.3V_t$ where V_t is the terminal velocity of 150µm polyethylene particle with density of 910g/cm^3. The geometry was a long pipe with funnel attached at the top of pipe. The pipe was 640 particle diameters tall and 20 particle diameters wide. Particles had initially a zero charge and 36410 particles were evenly distributed through out the fluidized bed.

We imposed an uniform superficial velocity boundary condition at the grate, and a constant pressure boundary condition at the outlet. The mesh was a hexahedra butterfly mesh with each cell having roughly three particle diameter witdth. This setup is was chosen to obtain grid independent CFDEM simulation.

The maximum particle charge was estimated from the charge transfer equation by setting the local electricfield term equal to the work function difference at the wall. This gave maximum charge q_{eq}

$$q_{eq} = \frac{2\pi\varepsilon_0}{\delta_c e}\Delta\phi r_i^2, \tag{21}$$

where δ_c is the electron cut-off distance, $\Delta\phi$ the work function difference between the particle and the wall which was varied between different simulation cases, and r_i particle radius.

In this study we studies monodisperse suspensions of particles that had $r_i = 150$µm and density similar to polyethylene 910kg/m^3.

We characterized the strength of the electrostatic effects by looking at the ratio of the electricfield at the contact of two particles with charge q_{eq} and the gravitational force. More formally we have

$$e/g = \frac{q_{eq}E}{mg}, \tag{22}$$

that becomes effectively a function of work function via Eq. (21). The cut-off radius of the electrostatic effects was chosen such that the electricfield coming from a particle with charge q_{eq} would be neglected when the force between two particles with charge q_{eq} was less than 10 percent from the gravitational force. The particles typically had charge less than q_{eq}, hence the 10 percent characterizes the largest possible cut-off error. The cut-off radius varied between 0.5 to 7 particle diameters in our simulations depending on the imposed work function difference. Six different work function cases were investigated, namely $e/g = 0$, $e/g = 0.1$, $e/g = 0.5$, $e/g = 1.0$, $e/g = 1.5$, and $e/g = 3.0$.

The tribocharging is generally a slow phenomenon, and takes minutes to hours to reach a steady state. To overcome this issue we accelerated the charge transfer by employing a coefficient similar to Eq. (20) that multiplied the charge transfer by 50.

Fig. 4 shows snapshots taken from the simulations. From the figure one can observe that the amount of particles sticking to the wall (green particles that have zero velocity) increases with increasing charge. Also the bed homogenuity increases with increasing charge, and there are no visible slugs in the highly charged cases. Interestingly, the

3.2 Tribocharging Rate

We computed the average charge on a particle at given time instance. As predicted by the Eq. (18), the charge increased by an exponential law, and approached the equilibrium charge. The charge evolution of the fluidized bed is shown in Fig. 5. The scaled total charge for all the three presented cases is very similar in the beginning of the simulations. However, once the particles charge the charging rate respect to equilibrium charge slows down. The charging rate decrease seems to be larger with larger charge.

One likely explanation for this is that the highly charged particles form a layer at the wall. This layer repels other charged particles ultimately decreasing the collision rate and collision velocity of these particles with the wall. Hence, in the highly charged cases this mechanism will cause increasing decrease in the charging rate as the particle charge increases.

Fig. 6 shows charging of the system with two different work function differences, and two different superficial velocities. The higher superficial velocity case charges slightly faster, but the difference is small. Hence, the superficial velocity had no major effects on the particle charging rate.

Fig. 7 shows the probability density functions of charge of the system with three different work function differences. As the work function values increase the distribution shifts to larger levels of charge. Interestingly, the density function also becomes wider, ans shows two separate peaks for the $e/g = 3$ case. To inspect this behavior further we computed charge distributions from particles that are in one diameter radius from wall, and the particles that are in the inner region. These results are shown in the Fig. 8. As can be seen from the figure, the particles at the wall have different density function than the particles at the inner region. The difference between the density functions increases with increasing charge leading to two separate peaks in the

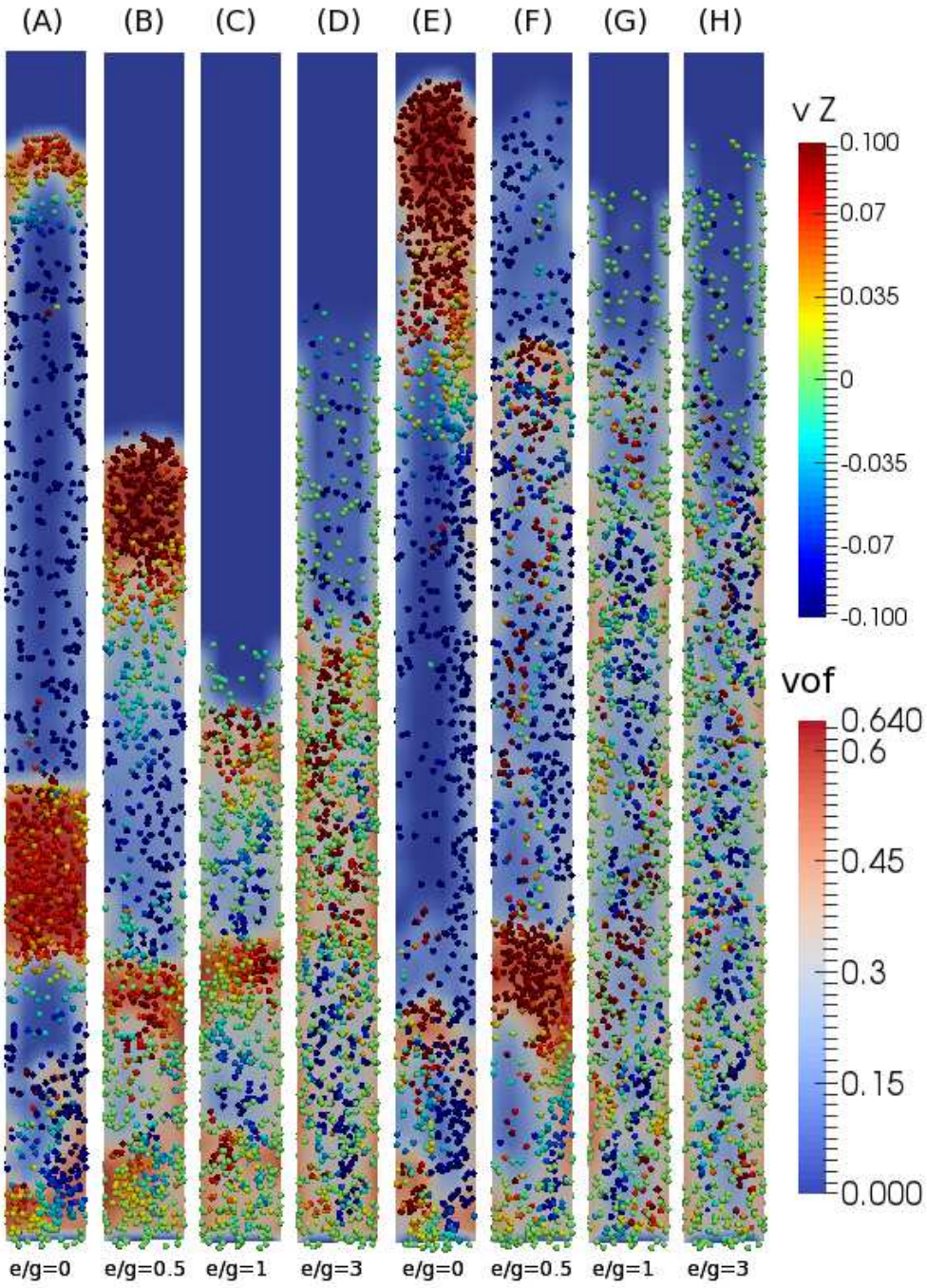

Figure 4: Snapshot taken at 1.8 s of eight different fluidization cases. Cases (A)-(D) have superficial velocity of $0.2V_t$ while cases (E)-(H) have superficial velocity of $0.3V_t$. The background is colored by the solids volume fraction, and particles are colored based on the vertical velocity. Every 20:th particle is shown in the figure from total of 36410 particles.

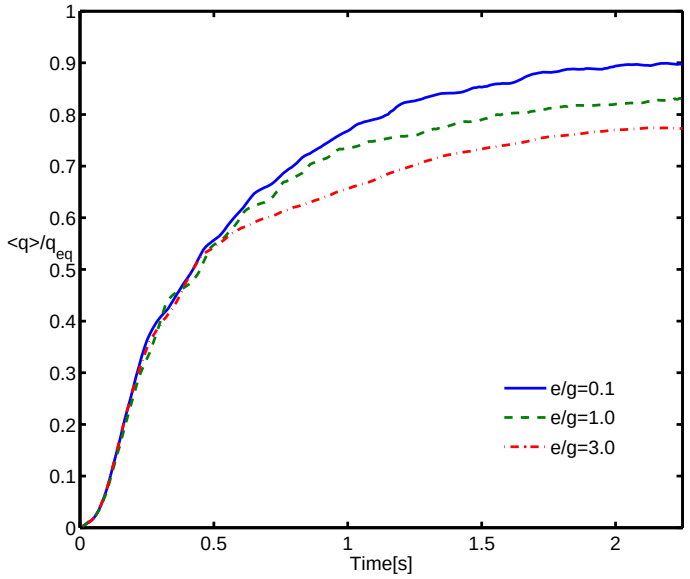

Figure 5: Charging rate of the fluidized bed with various rations of electrostatic forces to gravity.

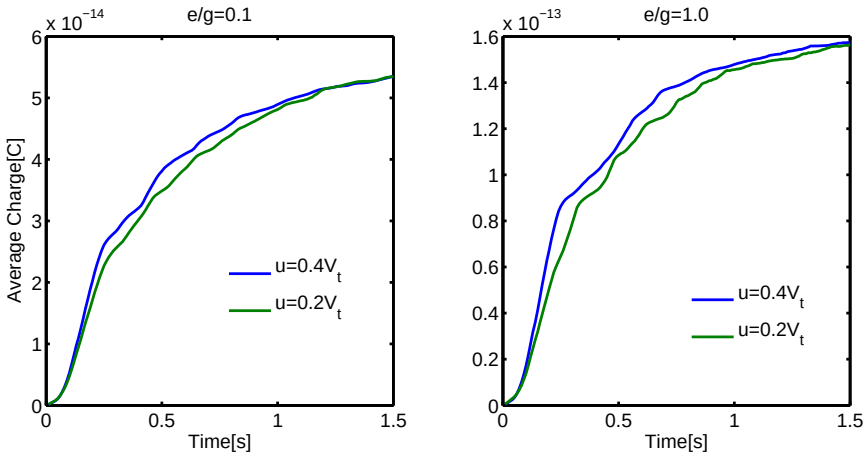

Figure 6: Charging rate of the fluidized bed with various two ratios of electrostatic forces to gravity, and varying superficial velocity.

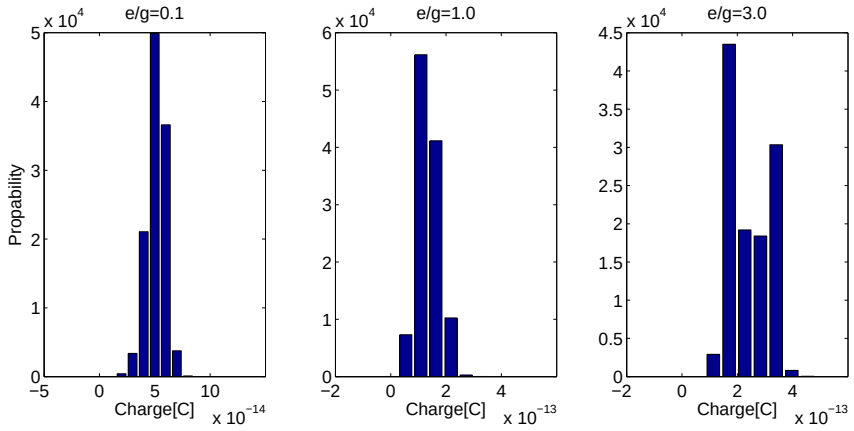

Figure 7: Probability distribution of charge.

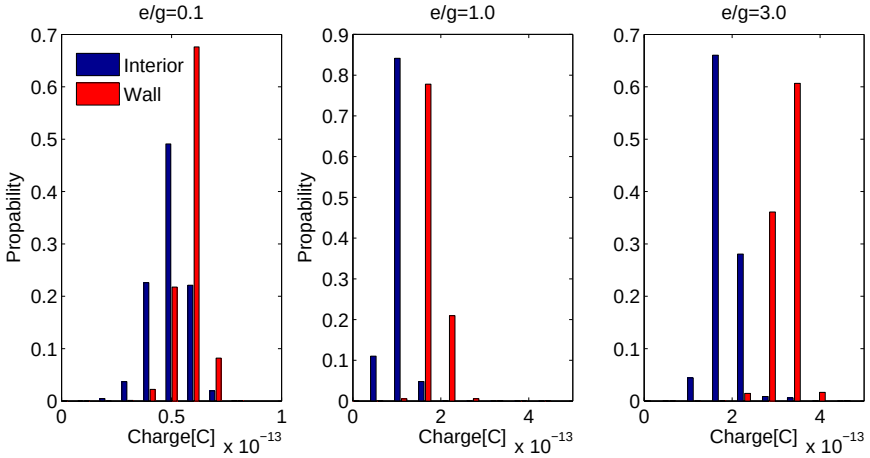

Figure 8: Probability distribution of charge respect to walls and interior.

case $e/g = 3$.

3.3 Particle Volume and Charge Distribution

The effect of charging to particle radial distribution and to radial charge distribution was investigated. These distributions were computed from time averages taken after the bed was reached to at least 70% percent from the equilibrium charge. The particle radial distribution is shown in Fig. 9. The charged particles tend to move at the wall due to attractive electrostatic force between the wall and the particles. Interestingly there is a low solid volume fraction area next to the wall. Possible cause for this could be the repeling force between the particles at the wall and particles approaching the wall which would also

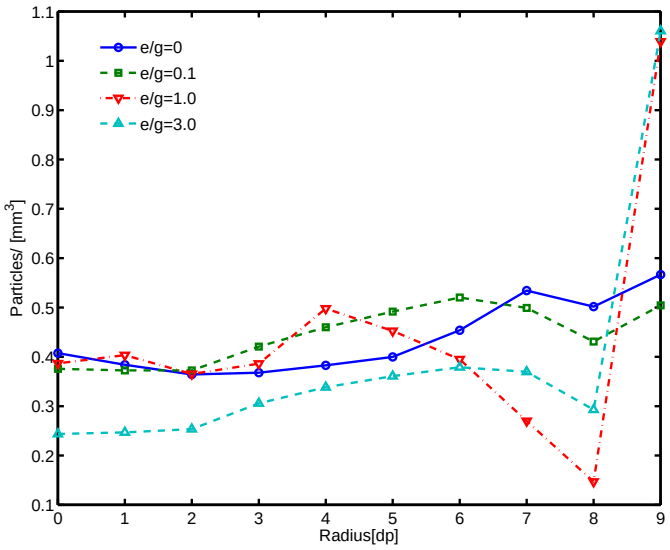

Figure 9: Radial particle distribution.

explain the decreases in the charging rate in Fig. 5. Fig. 10 shows fraction of the particles that is at the wall. We can see that the fraction increases to certain limit until the $e/g = 1$ case, and stays after that effectively constant. Furthermore, the higher superficial velocity has larger fraction of particles at the wall probably due to particles being able to also stick at the higher parts of the fluidized bed.

Fig. 11 shows the radial charge distribution for particle. The particles at the wall had the heighest charge, but interestingly the the particle charge decreased sharply after the wall, and started again slowly increasing. The possible cause for this behavior is that highly charged particles at the wall repel other particles with high charge. Hence it is more likely to find a particles with lower charge next to the wall layer than another particle with high charge. Authors believe that the gap between the interior and the wall might be effected by the high acceleration factor, since with low acceleration factor the particles would have more time to collide with the wall before they form the protective layer at the wall.

3.4 Particle Velocity Distribution

We computed the average particle velocity at different distances from particle center. The results are shown in Fig. 12. The lowly charged cases show particles moving up in the center of the bed, and falling

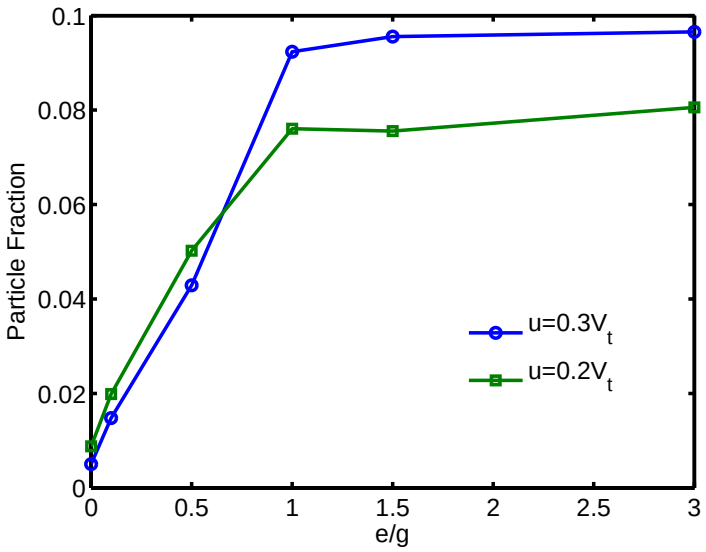

Figure 10: Particle fraction at the wall.

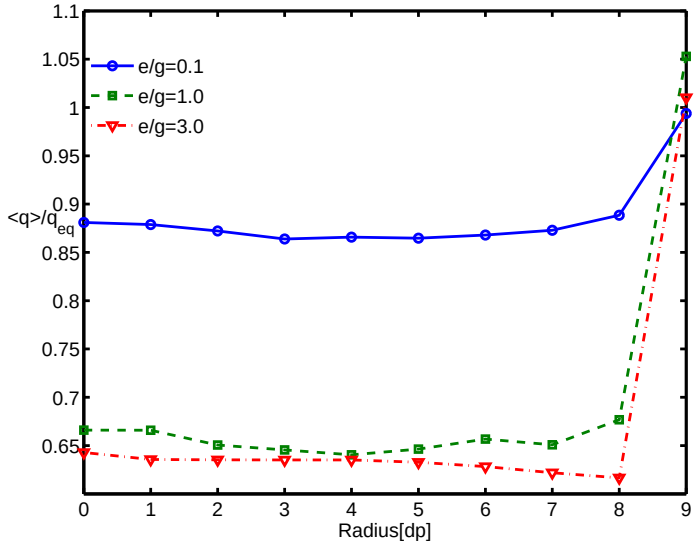

Figure 11: Radial average particle charge distribution.

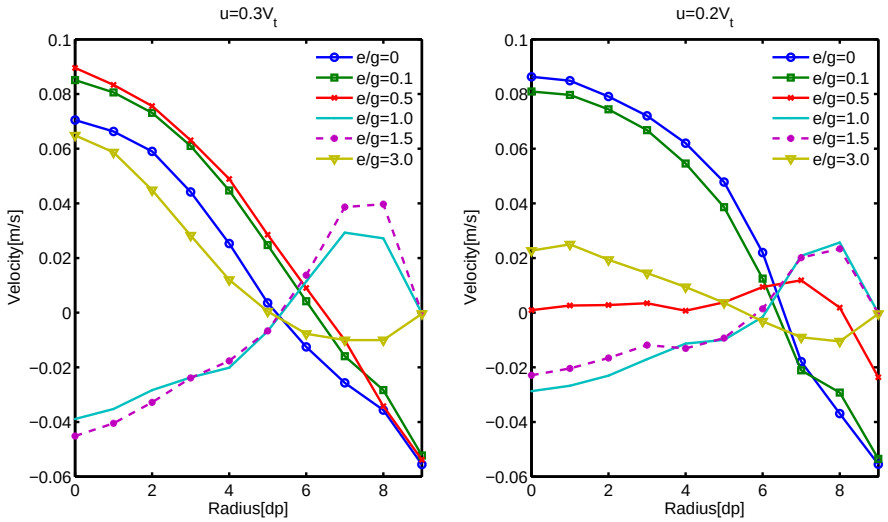

Figure 12: Time averaged vertical velocity distribution at different distances from the center of the bed. Various work function values and superficial velocities are shown.

down at the wall that is consistent with the uncharged case. However, when the charge on the particles increases the center of bed has a falling slug, and the intermediate particles next to the wall move up. This behavior could be caused by the reduced volume fraction next to the wall. Once the charge is increased even more, the bed returns to similar velocity distribution that the lowly charged cases have. It is also visible from the Fig. 12 that the particles form a static layer at the wall around $e/g = 1$ as the wall particle velocity goes effectively to zero.

3.5 Effects on Bed Height and to Pressure Loss

Fig. 13 shows bed heights at different times that contain 95% of the particles. The particles fall quicly to the hydrodynamical pseudo steady state. In the higher superficial gas velocity case, the bed height seems to be effected only slightly due to particle charging. However, the bed height oscillations are reduced clearly with the increasing charge. This is consistent with the prementioned observation of particles sticking at the wall and with the observation of Hassani [5] that monodispersed charged particles tend to produce more homogenous fluidization than uncharged particles.

For the lower superficial gas velocity case we also observe the decrease in the bed height oscillations, but also the bed height is de-

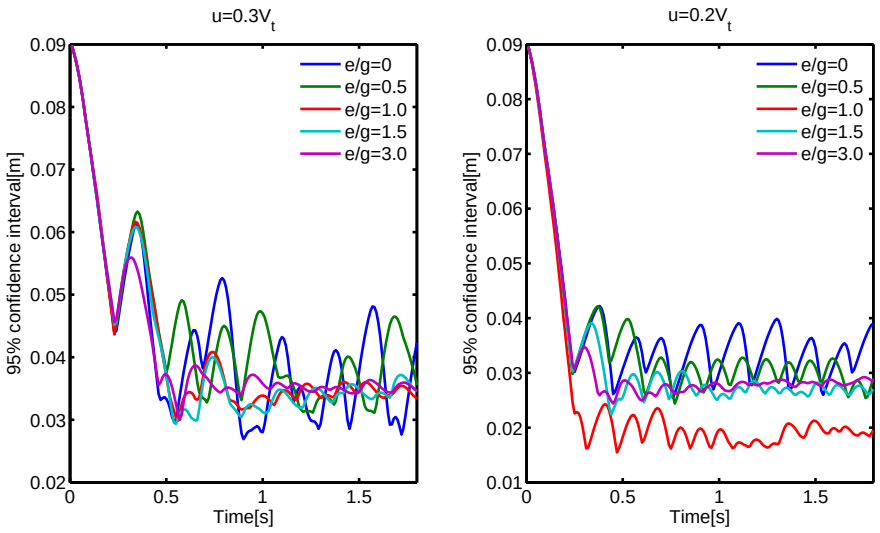

Figure 13: Figure showing instantenous bed heights that contain 95% of the particles.

creased with at first by increased particle charge, and then expanded again by increasing charge. This behavior can be explained by two mechanism: particle repelling force and particles sticking to the wall. When particles stick to the wall, the volume fraction in the center of the bed is decreased, and in-turn the particle drag is reduced. The reduced drag causes bed to collapse. When the particle charge is increased even further the repelling force of particles cause particles to stay farther away from each other. This will effectively cause the bed to expans and explains the increase seen form $e/g = 1$ to $e/g = 3$. The first case where particle sticking is observed is the case with $e/g = 1$, and we would expect a sudden drop at this point in the bed height that is visible in the lower superficial velocity case, but not with the higher superficial gas velocity.

The time averaged gas pressure curve at the center of the bed is shown in Fig. 14. The pressure loss over the bed decreases with with increasing particle charge.

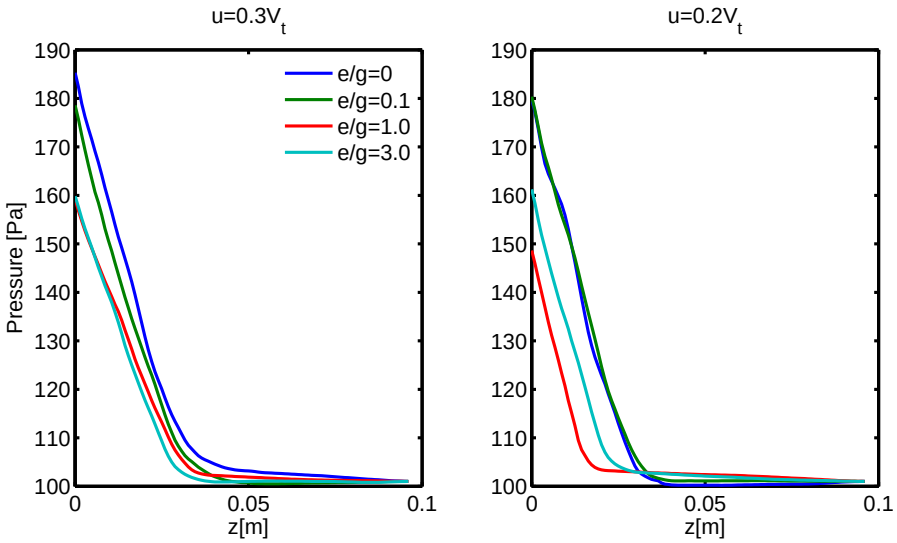

Figure 14: Time averaged pressure curves from bed bottom to the outlet with varying electrostatic force.

4 Conclusions

A: Parameters

Consider first the parameters α and β for two colliding particles. Assume that the colliding particles have initial charges q_{j0}, and q_{i0}, and work function difference $\Delta\phi$. Denote the transfered charge by $q_i(t)$ and $q_j(t)$, and let $t = 0$ stand for the beginning of the collision. The charge transfer rate is then given by

$$\frac{dq_i(t)}{dt} \propto \frac{\varepsilon}{\delta_c e}\left(\Delta\phi - \frac{\delta_c e}{4\pi\varepsilon}\left(\frac{q_{i0}+q_i(t)}{r_i^2} - \frac{q_{j0}+q_j(t)}{r_j^2}\right)\right). \tag{23}$$

For the charge rates we have

$$\begin{aligned}\frac{d}{dt}\left(q_i + q_j\right) &= \frac{dq_i}{dt} + \frac{dq_j}{dt} &(24)\\ &= \frac{dq_i}{dt} - \frac{dq_i}{dt} = 0. &(25)\end{aligned}$$

Hence, the charge is conserved and we may write

$$q_j(t) = q_i(0) + q_j(0) - q_i(t) = -q_i(t). \tag{26}$$

Inserting Eq. (26) to Eq. (23) we obtain

$$\frac{dq_i}{dt} \propto \frac{\varepsilon}{\delta_c e}\left(\Delta\phi - \frac{\delta_c e}{4\pi\varepsilon}\left(\frac{q_{i0}}{r_i^2} - \frac{q_{j0}}{r_j^2}\right) - \frac{\delta_c e}{4\pi\varepsilon}\left(\frac{1}{r_i^2} + \frac{1}{r_j^2}\right)q_i(t)\right). \tag{27}$$

We recognize that the α and β are now given by

$$\beta = \frac{\varepsilon}{\delta_c e}\left(\Delta\phi - \frac{\delta_c e}{4\pi\varepsilon}\left(\frac{q_{i0}}{r_i^2} - \frac{q_{j0}}{r_j^2}\right)\right) \tag{28}$$

and

$$\alpha = \frac{1}{4\pi}\left(\frac{1}{r_i^2} + \frac{1}{r_j^2}\right). \tag{29}$$

For the walls the charge transfer rate is obtained by mirroring the particle respect to wall, and assuming an imaginary charge that has equal charge with opposite sign in the other side of the wall. Hence we substitute for q_{j0}

$$q_{j0} = -q_{i0}. \tag{30}$$

Therefore, the α and β for the wall-particle collisions become

$$\beta = \frac{\varepsilon}{\delta_c e}\left(\Delta\phi - \frac{\delta_c e q_{i0}}{2\pi\varepsilon r_i^2}\right) \tag{31}$$

and

$$\alpha = \frac{1}{2\pi r_i^2}. \tag{32}$$

B: Contact Area

The contact area in the softsphere model is given by

$$A_{max} = \pi\delta_{max}\frac{r_i r_j}{r_i + r_j}, \tag{33}$$

where δ_{max} is the maximum overlap distance, r_i and r_j are the particle radiuses. The overlap δ_{max} for similarly sized particles satisfies

$$\delta_{max} \ll (r_i + r_j)\frac{r_i}{r_j}. \tag{34}$$

The coefficient α can be writen as

$$\alpha = \frac{1}{4\pi}\frac{r_i^2 + r_j^2}{r_i^2 r_j^2}. \tag{35}$$

Consider first a collision between two particles

$$\begin{aligned}
\alpha A_{max} &= \frac{1}{4\pi}\frac{r_i^2 + r_j^2}{r_i^2 r_j^2}\pi\delta_{max}\frac{r_i r_j}{r_i + r_j} && (36)\\
&= \frac{1}{4}\left(\frac{r_i\delta_{max}}{r_j(r_i + r_j)} + \frac{r_j\delta_{max}}{r_i(r_i + r_j)}\right) && (37)\\
&\ll \frac{1}{4}(1 + 1) < 1. && (38)
\end{aligned}$$

For wall collisions the the overlap distance satisfies $\delta_{max} \ll r_i$, hence

$$\begin{aligned}
\alpha A_{max} &= \frac{1}{2\pi r_i^2}\pi\delta_{max} r_i && (39)\\
&= \frac{\delta_{max}}{2r_i} && (40)\\
&\ll \frac{1}{2} < 1. && (41)
\end{aligned}$$

References

[1] Nathan Duff and Daniel J. Lacks. Particle dynamics simulations of triboelectric charging in granular insulator systems. *Journal of Electrostatics*, 66(12):51–57, January 2008.

[2] Keith M. Forward, Daniel J. Lacks, and R. Mohan Sankaran. Charge Segregation Depends on Particle Size in Triboelectrically Charged Granular Materials. *Physical Review Letters*, 102(2):028001, January 2009.

[3] Rubia F. Gouveia and Fernando Galembeck. Electrostatic Charging of Hydrophilic Particles Due to Water Adsorption. *Journal of the American Chemical Society*, 131(32):11381–11386, August 2009.

[4] W.R. Harper. *Contact and Frictional Electrification*. PhD thesis, Oxford, 1967.

[5] M. A. Hassani, R. Zarghami, H. R. Norouzi, and N. Mostoufi. Numerical investigation of effect of electrostatic forces on the hydrodynamics of gassolid fluidized beds. *Powder Technology*, 246:16–25, September 2013.

[6] Gregory Hendrickson. Electrostatics and gas phase fluidized bed polymerization reactor wall sheeting. *Chemical Engineering Science*, 61(4):1041–1064, February 2006.

[7] Farzaneh Jalalinejad. Electro-hydrodynamics of gas-solid fluidized beds. 2013.

[8] Farzaneh Jalalinejad, Xiaotao T. Bi, and John R. Grace. Effect of electrostatic charges on single bubble in gassolid fluidized beds. *International Journal of Multiphase Flow*, 44:15–28, September 2012.

[9] Farzaneh Jalalinejad, Xiaotao T. Bi, and John R. Grace. Effect of electrostatics on interaction of bubble pairs in a fluidized bed. *Advanced Powder Technology*, 26(1):329–334, January 2015.

[10] Thomas B. Jones and Jack L. King. *Powder Handling and Electrostatics*. Lewis Publishers Inc., 1991.

[11] Jasper F. Kok and Daniel J. Lacks. Electrification of granular systems of identical insulators. *Physical Review E*, 79(5):051304, May 2009.

[12] Daniel J Lacks and R Mohan Sankaran. Contact electrification of insulating materials. *Journal of Physics D: Applied Physics*, 44(45):453001, November 2011.

[13] J. C. Laurentie, P. Traor, and L. Dascalescu. Discrete element modeling of triboelectric charging of insulating materials in vibrated granular beds. *Journal of Electrostatics*, 71(6):951–957, December 2013.

[14] J.-C. Laurentie, P. Traor, C. Dragan, and L. Dascalescu. Numerical Modeling of Triboelectric Charging of Granular Materials in Vibrated Beds. In *2010 IEEE Industry Applications Society Annual Meeting (IAS)*, pages 1–6, October 2010.

[15] LoganS. McCarty and GeorgeM. Whitesides. Electrostatic Charging Due to Separation of Ions at Interfaces: Contact Electrification of Ionic Electrets. *Angewandte Chemie International Edition*, 47(12):2188–2207, March 2008.

[16] Ram G. Rokkam, Rodney O. Fox, and Michael E. Muhle. Computational fluid dynamics and electrostatic modeling of polymerization fluidized-bed reactors. *Powder Technology*, 203(2):109–124, November 2010.

[17] Andrew Sowinski, Leigh Miller, and Poupak Mehrani. Investigation of electrostatic charge distribution in gassolid fluidized beds. *Chemical Engineering Science*, 65(9):2771–2781, May 2010.

[18] Huiliang Zhao, G.S.P. Castle, I.I. Inculet, and A.G. Bailey. Bipolar charging of poly-disperse polymer powders in fluidized beds. *IEEE Transactions on Industry Applications*, 39(3):612–618, May 2003.